Draft version February 14, 2007
Preprint typeset using LaTeX style emulateapj v. 10/09/06

arXiv:astro-ph/0702321v1 12 Feb 2007

MODELING LYMAN CONTINUUM EMISSION FROM YOUNG GALAXIES

Alexei O. Razoumov[1] and Jesper Sommer-Larsen[2]

Draft version February 14, 2007

ABSTRACT

Based on cosmological simulations, we model Lyman continuum emission from a sample of 11 high-redshift star forming galaxies spanning a mass range of a factor 20. Each of the 11 galaxies has been simulated both with a Salpeter and a Kroupa initial mass function (IMF). We find that the Lyman continuum (LyC) luminosity of an average star forming galaxy in our sample declines from $z = 3.6$ to 2.4 due to the steady gas infall and higher gas clumping at lower redshifts, increasingly hampering the escape of ionizing radiation. The galaxy-to-galaxy variation of apparent LyC emission at a fixed redshift is caused in approximately equal parts by the intrinsic variations in the LyC emission and by orientation effects. The combined scatter of an order of magnitude can explain the variance in the far-UV spectra of high-redshift galaxies detected by Shapley et al. (2006). Our results imply that the cosmic galactic ionizing UV luminosity would be monotonically decreasing from $z = 3.6$ to 2.4, curiously anti-correlated with the star formation rate in the smaller galaxies, which on average rises during this redshift interval.

Subject headings: galaxies: formation — intergalactic medium — HII regions — radiative transfer

1. INTRODUCTION

Recent spectroscopic detection of Lyman continuum (LyC) emission from individual $z \sim 3$ galaxies (Shapley et al. 2006) represents a major step forward in analyzing the stellar contribution to the ionizing background at high redshifts. In a study of 14 $z \sim 3$ star-forming (SF) galaxies Shapley et al. (2006) have detected escaping ionizing radiation from two objects, concluding that there is significant variance in the emergent LyC spectrum. The nature of this variance is currently not understood, although it is undoubtedly linked to the physical conditions in the interstellar medium (ISM) at these high redshifts. Comparison of observed LyC emission to theoretical models should in principle allow us to put constraints on the physics of SF in young galaxies and study the effect of stellar radiation on the thermal properties of high-redshift gas, including its role in maintaining cosmic reionization. One of the main parameters in this study is the escape fraction of ionizing photons from the clumpy ISM, a quantity of primary importance in determining the contribution of the volumetric stellar luminosity to the ionizing background.

In Razoumov & Sommer-Larsen (2006, Paper I) we presented calculations of the escape fraction of LyC photons from a large number of SF regions in two simulated high-redshift proto-galaxies. We found that the modeled redshift evolution of $f_{\rm esc}$ matches the observational findings of Inoue et al. (2006), namely the decline from $f_{\rm esc} \sim 6-10\%$ at $z \gtrsim 3.6$ to $f_{\rm esc} \sim 1-2\%$ at $z = 2.4$. This decline is attributed to a much higher clustering of gas around the SF regions at lower redshifts, due to accretion of the intergalactic gas onto growing proto-galaxies. In this paper we extend these calculations to a larger set of (proto-) spiral galaxies covering a range of masses and study the dependence of our results on the amount of feedback per unit stellar mass encoded in the initial mass function (IMF). We moreover determine galaxy-to-galaxy LyC emission variations at a given redshift and galaxy mass, as well as variations for a given galaxy along different lines of sight.

Electronic address: razoumov@ap.smu.ca
Electronic address: jslarsen@dark-cosmology.dk
[1] Institute for Computational Astrophysics, Dept. of Astronomy & Physics, Saint Mary's University, Halifax, NS, B3H 3C3, Canada
[2] Dark Cosmology Centre, Niels Bohr Institute, University of Copenhagen, Juliane Maries Vej 30, DK-2100 Copenhagen, Denmark

2. MODELS

We use results of high-resolution galaxy formation simulations in a standard LCDM cosmology done with a significantly improved version of the TreeSPH code described by Sommer-Larsen et al. (2003) – more details on this simulation set are provided in Sommer-Larsen (2006). Table 1 lists 11 galaxies, in order of increasing mass, for which we performed radiative transfer calculations around all their SF regions at $z = 3.6$, 2.95 and 2.39. The first five are fairly small ($V_{\rm c} \lesssim 130\,{\rm km\,s^{-1}}$, see below), gas-rich galaxies that exhibit relatively little SF. Galaxy 41 is an intermediate-size system with $V_{\rm c} = 150\,{\rm km\,s^{-1}}$, whereas the rest are larger ($V_{\rm c} \gtrsim 180\,{\rm km\,s^{-1}}$) disk galaxies. The most massive galaxies were computed at "normal" resolution, with SPH (and star) particle masses of $1.1 \times 10^6\,{\rm M_\odot}$ and interpolated grid resolution of 30 pc, the smaller galaxies were simulated with 8 times higher mass resolution and twice the force resolution. The only "low" resolution simulation was the $V_{\rm c} = 310\,{\rm km\,s^{-1}}$ galaxy with particle masses of $3.1 \times 10^6\,{\rm M_\odot}$.

All galaxies in Table 1 are labeled by their $z = 0$ characteristic circular velocities, which were calculated using the technique described in Sommer-Larsen & Dolgov (2001). For our purpose, the present-day $V_{\rm c}$ is a good measure of $z \sim 3$ galaxy masses for a number of reasons. First, galaxies tend to grow in size from $z = 3$ to $z = 0$, but not so much in $V_{\rm c}$. In addition, there is a fairly tight relation between the $z = 3$ stellar and virial masses and the $z = 0$ ones. This is simply explained by the fact that our sample contains only field galaxies, which become disks by $z = 0$. All of them have relatively quiet $z < 3$

TABLE 1
GALAXY PAIRS SALPETER – KROUPA.

Galaxy	resolution	V_c(z=0) $\mathrm{km\,s^{-1}}$	comment
84	high	115	small galaxy
93	high	122	same
115	high	125	same
108	high	131	same
87	high	132	same
41	normal	150	intermediate-size
33	normal	180	sub-Milky Way
29	normal	205	slightly sub-Milky Way
26	normal	208	same
15	normal	245	M31-like disk galaxy
15_sc1.39	low	310	very large disk galaxy

merging histories; in fact, at $z = 3$ it is already fairly easy to identify the main proto-galaxy. Finally, most of our $z = 3$ systems have several proto-galactic components, and our results at $r = 100\,\mathrm{kpc}$ account for absorption and stellar emission in all of these components, not just the main proto-galaxy.

We model SF with a set of discrete star "particles", which represent a population of stars born at almost the same time in accordance with a given IMF. To compute the time-dependent ionization by UV photons from the local star forming regions, we use the point source radiative transfer algorithm on adaptively refined meshes first employed in Paper I. The stellar UV luminosity is determined using the population synthesis package Starburst 1999 (Leitherer et al. 1999) with continuous SF distributed among all stars younger than 34 Myrs.

To study the sensitivity of our results to the strength of stellar feedback which is in turn a function of the number of massive stars in our SF regions, we adopt two different but widely used IMFs, the standard Salpeter (1955) and the triple-interval Kroupa (1998) IMF. The Salpeter IMF produces approximately twice as much SNII feedback and stellar ionizing radiation per unit stellar mass compared to the Kroupa IMF. However, both IMFs result in less feedback than the more top-heavy IMF used in Paper I. The SNII feedback and chemical enrichment are included into the hydrodynamical models, whereas the propagation of ionizing stellar photons is traced with post-process radiative transfer, as detailed in Paper I.

3. RESULTS

3.1. *Dependence on the amount of massive stars*

Following Paper I, we define $f_{\rm esc}$ simply as the fraction of (ionizing) stellar photons of a given frequency that reach distance r from the SF regions. Here all our results are computed at $r = 100\,\mathrm{kpc}$, unless stated otherwise, at $t = 10\,\mathrm{Myrs}$ after the stellar sources were switched on. However, to obtain these solutions, the full 3D time-dependent ionization structure of the gas was computed. Our results are fairly robust to changes in the numerical resolution, as it was shown in Paper I.

In Fig. 1 we plot the angle- and source-averaged escape fractions for all galaxies from Table 1 as a function of the photon energy, at $z = 3.6$, 2.95 and 2.39. We confirm our earlier conclusion (Razoumov & Sommer-Larsen 2006) that $f_{\rm esc}$ shows tendency to decrease with time due to increased clustering of gas near the SF regions. However, there are a few exceptions at later times – the more massive galaxies 33, 29, 26 with the Salpeter IMF show-

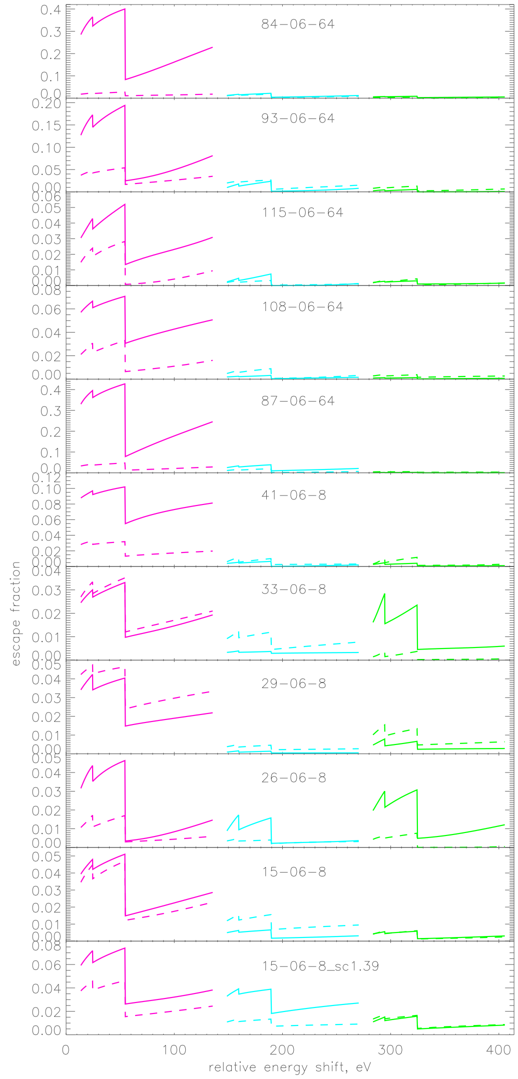

FIG. 1.— Spectral dependence of $f_{\rm esc}$ at $r = 100\,\mathrm{kpc}$ for all Salpeter (solid lines) – Kroupa (dashed lines) galaxy pairs at $z = 3.6$ (magenta), $z = 2.95$ (cyan), and $z = 2.39$ (green). For each model the redshift evolution is from left to right, and each curve goes from 13.6 eV to 135 eV. Galaxies are listed in order of increasing mass (top to bottom).

ing a rise in $f_{\rm esc}$ from $z = 2.95$ to 2.39. Overall, we find significant variations from galaxy to galaxy, especially in the lower-mass systems, with the Salpeter IMF Lyman-limit $f_{\rm esc}$ varying from 3% in 115 to 33% in 87.

Sommer-Larsen et al. (2003) found that early, fairly strong bursts of SF converting several percent of the initial gas mass into stars can substantially alleviate the disk galaxy angular momentum problem, as feedback from these starbursts can blow a larger fraction of the remaining gas out of the small proto-galactic clumps, with this gas later gradually settling to form extended disks. With the Salpeter IMF the stronger feedback at early times suppresses SF relative to the Kroupa case yielding less massive $z \sim 3$ stellar components (Fig. 2), and building up a larger reservoir of hot gas around the galaxy. This results in an anti-correlation between $f_{\rm esc}$ and the number of young ($t_{\rm age} < 34\,\mathrm{Myrs}$) stars at $z = 3.6$ (Fig. 3): the stronger feedback there is in a galaxy, the fewer stars it forms, but also the higher $f_{\rm esc}$

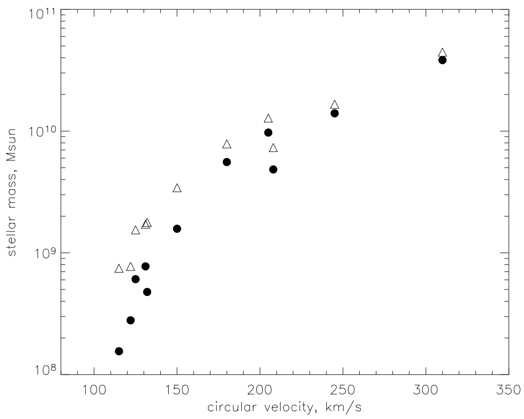

FIG. 2.— Total $z = 3$ stellar mass vs. the characteristic circular velocity for Salpeter (filled circles) and Kroupa (open triangles) galaxies.

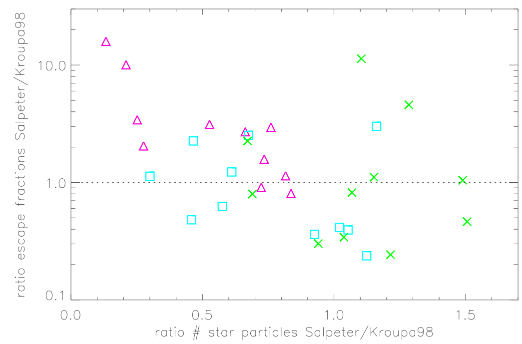

FIG. 3.— Ratio $f_{\rm esc,S}/f_{\rm esc,K}$ of the Lyman-limit escape fractions for models with the Salpeter and Kroupa IMFs vs. the ratio $N_{*,\rm S}/N_{*,\rm K}$ of the number of young ($t_{\rm age} < 34\,$Myrs) stellar particles in each pair of models, at $z = 3.6$ (magenta), $z = 2.95$ (cyan), and $z = 2.39$ (green).

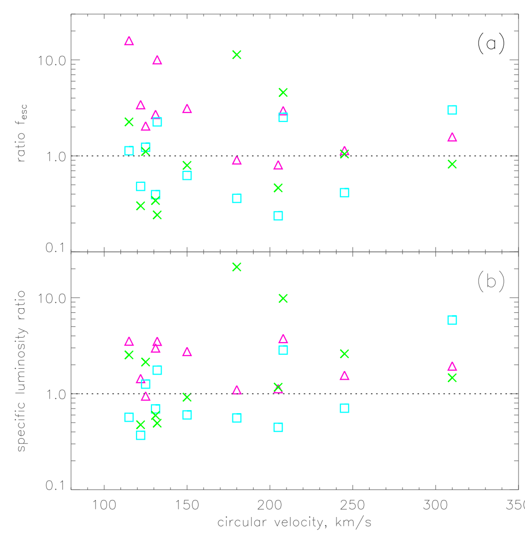

FIG. 4.— Ratio $f_{\rm esc,S}/f_{\rm esc,K}$ of the Lyman-limit escape fractions (a) and the Lyman-limit specific luminosities (b) for models with the Salpeter and Kroupa IMFs vs. the characteristic circular velocity, at $z = 3.6$ (magenta), $z = 2.95$ (cyan), and $z = 2.39$ (green).

it gets as the same amount of gas is being dispersed over a larger volume, and more neutral gas is ionized per unit stellar mass. This anti-correlation reduces the sensitivity of the absolute UV luminosity to the fraction of massive stars encoded in the IMF. For example, in galaxy 87 ($v_c = 132\,{\rm km\,s^{-1}}$) at $z = 3.6$ its Salpeter $f_{\rm esc}$ is about 10 higher than the Kroupa $f_{\rm esc}$ (Fig. 4a), however, it has 93 young stellar particles with the Salpeter IMF, while the Kroupa IMF results in 444 particles. The result is that its Salpeter luminosity is only ~ 3 times higher than its Kroupa luminosity (Fig. 4b).

Eventually, the feedback cannot prevent the cool-out of hot gas, which sooner or later leads to a rise in SF. In fact, Salpeter galaxies tend to produce more stars than Kroupa galaxies at later times, as can be seen in the number of young stars along the horizontal axis in Fig. 3 at $z = 2.39$. By this time, however, there is no correlation between the escape fractions and the number of recent starbursts, as consistently stronger feedback has a very non-linear effect on the gas distribution at lower redshift. On one hand, models with higher feedback rates per unit stellar mass generally have more gas left over for SF from earlier times, and by $z = 2.39$ some of this gas might have cooled back into dense clouds in the disk ISM. Therefore, combined supernova winds now have to push through a thicker layer of material, unless all of this cool-out gas has been efficiently converted into stars on a short timescale which is unlikely. On the other hand, irrespective of the earlier SF history, stronger feedback might still clear channels through which ionizing photons escape into the intergalactic medium. The end result is that all these processes create a very complex porous ISM, with lower average $f_{\rm esc}$, but higher variations from galaxy to galaxy, and a larger scatter when we vary the IMF (Fig. 4a,b), as by now many effects contribute to the value of $f_{\rm esc}$.

Gas blowout is expected to be less efficient in already formed disk galaxies as it drives a typically much smaller fraction of interstellar gas in bipolar outflows perpendicular to the disk (Mac Low & Ferrara 1999). As one would expect, in our models the escape fractions show a weaker dependence on the feedback strength in the most massive galaxies (Fig. 4a).

The luminosity of each galaxy is a product of the original IMF spectrum, the number of SF regions in the galaxy, the SF rate of each region which depends on the mass of a stellar particle, and the escape fraction. In Fig. 5 we plot the specific (per unit frequency) Lyman-limit luminosity L_{912} of each galaxy vs. its circular velocity, at all three redshifts. Overall, the Lyman-limit luminosities of galaxies simulated using the two different IMFs follow similar trends with $V_{\rm c}$ and z. Note that for most systems L_{912} is higher at earlier times, meaning that galaxies become an increasingly more important source of ionizing photons relative to quasars the number density of which declines rapidly at $z \gtrsim 3$ (Richards et al. 2006). Therefore, the results shown in Fig. 5 are of great importance in relation to the ionization history of the Universe, and we shall return to this topic in a forthcoming paper.

We also find that the average cosmic galactic LyC luminosity which in our models decreases monotonically from $z = 3.6$ to 2.4, most notably in the low mass galaxies, is anti-correlated with the star formation rate in the same galaxies, which rises during this redshift interval. For the 5 small ($V_{\rm c} < 150\,{\rm km\,s^{-1}}$) galaxies in our sample, the average SF rates are 1.8, 2.6 and 2.7 $M_\odot\,{\rm s^{-1}}$ at $z = 3.6$,

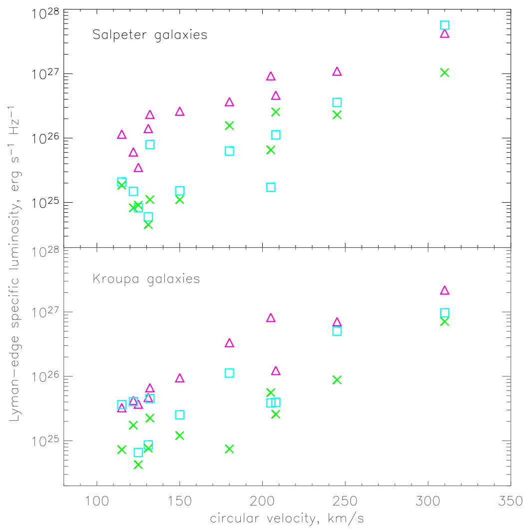

FIG. 5.— Lyman-limit specific luminosity vs. the characteristic circular velocity, at $z = 3.6$ (magenta), $z = 2.95$ (cyan), and $z = 2.39$ (green), for Salpeter (top) and Kroupa (bottom) galaxies.

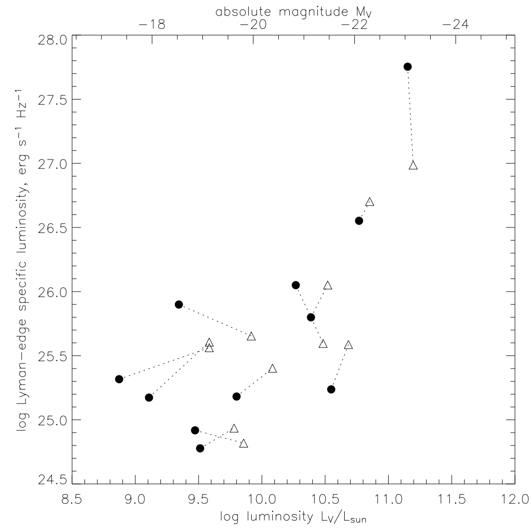

FIG. 6.— Lyman-limit specific luminosity at $z = 2.95$ vs. the optical luminosity. The dotted lines connect a pair of models of each galaxy evolved with the Salpeter (filled circles) and Kroupa (open triangles) IMFs, respectively. The logarithmic scale is the same on the vertical and horizontal axes.

2.95 and 2.39 for the Kroupa galaxies, and 0.6, 1.4 and 2.8 $\mathrm{M}_\odot\,\mathrm{s}^{-1}$ for the Salpeter galaxies, respectively. For the larger galaxies, the evolution of the SF rate with redshift is more flat in the $z = 3.6 - 2.4$ interval. Both above findings are in qualitative agreement with the observational result of Sawicki & Thompson (2006), that the galaxy (non-ionizing) UV luminosity function gradually rises at the faint end from $z = 4$ to $z = 2$, while the bright end of the luminosity function exhibits virtually no evolution.

In Fig. 6 we plot the Lyman-limit luminosities of all galaxies in our sample vs. their optical luminosities, at $z = 2.95$. The optical luminosity is tightly coupled to the number of bright stars, whereas the ionizing luminosity also depends on the amount of absorbing neutral gas in the vicinity of SF regions. As gas blowout is less efficient in more massive galaxies, the supply of material available for SF does not depend so strongly on the feedback strength, and the optical luminosity of such galaxies is less affected when varying the IMF. The ionizing luminosities, on the other hand, are sensitive to the conditions near SF regions and show variations even in already formed massive systems. It is also seen from Fig. 6 that the effects of changing the IMF on the LyC and optical luminosities, respectively, are essentially uncorrelated.

3.2. *Radial dependence of the escape fraction*

To probe conditions inside the ISM, it is instructive to look at the radial dependence of absorption as a function of redshift in one of our galaxies. In Fig. 7 we show the 4π-averaged distribution of $f_{\rm esc}$ for all star particles in the more massive galaxy 15, computed with the Kroupa IMF, as a function of redshift and the distance from these particles. At all five redshifts a significant fraction of photons reaches the radius $r = 100\,\mathrm{pc}$, although this fraction decreases with time as more gas is clustered around the SF regions. At $r = 1\,\mathrm{kpc}$ the redshift evolution is more noticeable, as very few sources have $f_{\rm esc} > 0.1$ at $z = 2.39$. As a result, beyond this galaxy's virial radius of $r \sim 45\,\mathrm{kpc}$, the average Lyman-limit escape fraction drops from $\sim 4\%$ to $\sim 0.4\%$ in the above redshift interval.

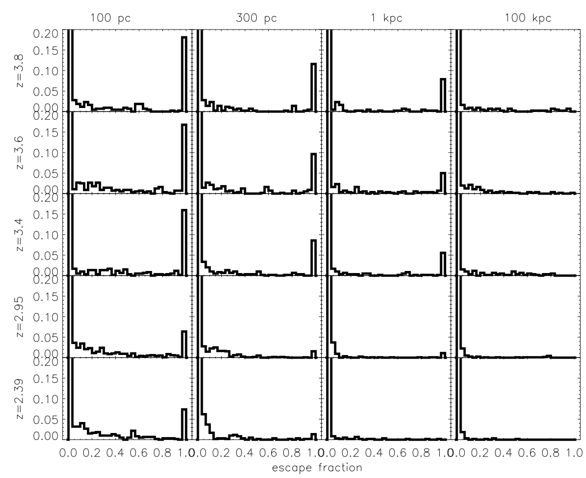

FIG. 7.— Distribution of sources by their Lyman-limit escape fractions in galaxy 15 with the Kroupa IMF at $z = 3.8$, 3.6, 3.4, 2.95 and 2.39 (top to bottom), at four different radii, from 100 pc to 100 kpc (left to right). The vertical axis has been truncated to showcase the radial distribution.

3.3. *Orientation effects*

In Section 3.1 we saw that for galaxies of a given mass the galaxy-to-galaxy scatter in the LyC emission can be partially attributed to variations in the physical conditions in the clumpy ISM *surrounding* the SF regions (factor of $\sim 2 - 3$ for either of the selected IMFs in Fig. 5).

In this section we examine variations in *apparent* LyC luminosities caused by orientation effects, i.e. that galaxies will be oriented in a random way with respect to an observer. The source-to-source scatter in $f_{\rm esc}$ (Fig. 7) and a non-uniform gas distribution in host galaxies invariably translate into angular variations. In Fig. 8–9 we plot the angular dependence of $f_{\rm esc}$ for two galaxies, the more massive 15 and the small 93, at three different redshifts, both galaxies computed with the Kroupa IMF. For Salpeter galaxies the behaviour is qualitatively the

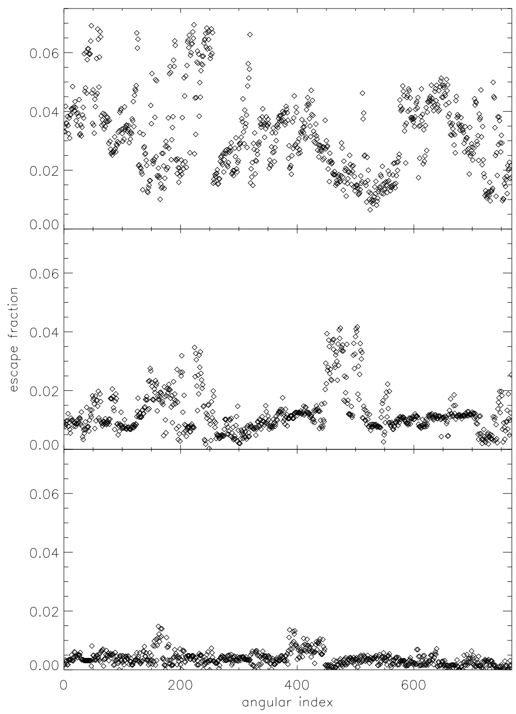

FIG. 8.— Angular variation of the Lyman-limit escape fraction for K15, at $z = 3.6$, 2.95, and 2.39 (top to bottom).

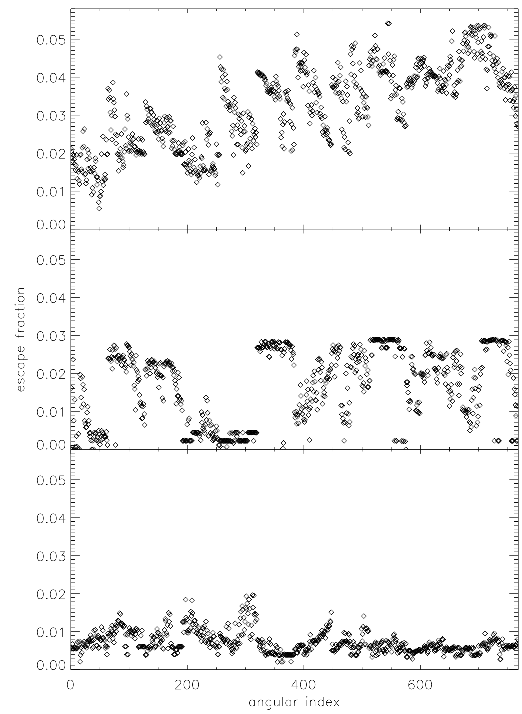

FIG. 9.— Same as Fig. 8, but for K93.

same. In both plots the x-axis gives the index of the angular pixel in the Healpix (Górski et al. 2002) notation, covering the entire 4π in $768 = 12 \times 4^3$ bins. Essentially, it is as an index along a fractal space-filling curve going through all bins on the sky (as seen from the galaxy) in which $f_{\rm esc}$ was computed, with each bin covering the same solid angle. For the more massive galaxy 15, especially with the Kroupa IMF, we can see two spikes corresponding to the face-on orientation of the galaxy, with $f_{\rm esc} \sim 2-3$ times the average.

In Fig. 10 we plot the angular probability distribution function of $f_{\rm esc}$ for two Salpeter and two Kroupa galaxies, at all three redshifts. The vertical axis shows the fraction of angular bins per unit log $f_{\rm esc}$, such that the area under each curve is exactly unity. The decline of $f_{\rm esc}$ with time is evident in all four panels, but more interesting is the scatter of about an order of magnitude in $f_{\rm esc}$ depending on orientation to the observer. This, together with the intrinsic LyC luminosity variation from galaxy to galaxy (Fig. 5) explains why in magnitude-limited surveys only a fraction of galaxies are detected in direct LyC emission (Shapley et al. 2006).

4. CONCLUSIONS

In conclusion, we presented calculations of the LyC emission from 11 (proto-) disk galaxies in the redshift range $z = 3.6 - 2.4$, modeled with the standard Salpeter and Kroupa IMFs. To calculate the ionization structure of the interstellar medium in each galaxy, we performed time-dependent numerical radiative transfer around a large number (up to 10^4) of SF regions modeled with discrete star particles. Our findings are as follows:

1) Although we find significant variations in the escape fraction of ionizing photons from galaxy to galaxy, we confirm our earlier results on the average decrease of $f_{\rm esc}$ from $z = 3.6$ to 2.4 for the entire range of galaxy masses, as more gas cools and accretes onto galaxies, forming stars in progressively clumpier environments. The resulting LyC luminosity of individual galaxies declines gradually over this redshift interval, by nearly an order of magnitude for lower-mass galaxies, and a smaller factor

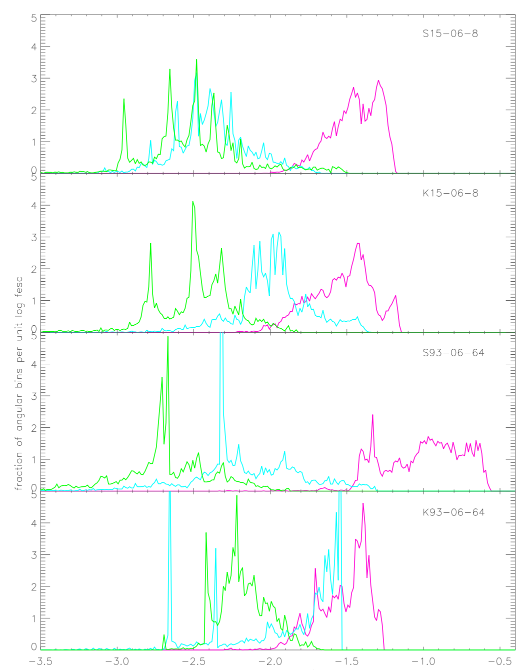

FIG. 10.— Probability function of the angular distribution of the Lyman-limit escape fraction for galaxies 15 and 93 at $z = 3.6$ (magenta), $z = 2.95$ (cyan), and $z = 2.39$ (green), with Salpeter and Kroupa IMFs as indicated in each panel.

for more massive objects. We also note that this result is not sensitive to the assumed IMF, at least within the range of feedback parameters normally associated with the widely used Salpeter and Kroupa IMFs.

2) The observed galaxy-to-galaxy scatter in LyC emission is caused in approximately equal parts by the inclination effects and the intrinsic variations in the 4π-averaged UV luminosities, for galaxies of a fixed mass. Effects of dust extinction have not been included into our calculations, but it is likely that such effects will increase the galaxy-to-galaxy LyC luminosity scatter, as seen by a given observer, even further.

3) We predict that the cosmic galactic ionizing UV luminosity would be monotonically decreasing from $z = 3.6$ to 2.4. Some fraction of smaller galaxies in clusters can turn on their SF for the first time during this redshift interval due to tidal effects, however, the intrinsic changes in most field galaxies associated with continuous gas infall would lead to a decline in the LyC comoving luminosity density.

On the other hand, there is evidence that the galaxy non-ionizing UV luminosity function gradually rises at the faint end from $z = 4$ to $z = 2$ (Sawicki & Thompson 2006). We want to stress that our findings do not contradict these data, as indeed we see a rise by a factor of $\sim 2 - 4$ in the number of young stars from $z = 3.6$ to 2.4 in all our small galaxies, consistent with continuous gas infall. We are planning to study the non-ionizing UV luminosity function in the same set of galaxies in the future.

4) The higher escape fractions as well as LyC luminosities found at $z = 3.6$, compared to the lower redshifts, also support the notion that galaxies become a progressively more important source of ionizing photons as one goes back in time, as the comoving number density of quasars declines rapidly at $z \gtrsim 3$ (Richards et al. 2006).

We wish to thank Akio Inoue for drawing our attention to the question of dispersion of observed $f_{\rm esc}$ along various lines of sight, and Marcin Sawicki for careful reading of the manuscript. Numerical calculations were done on the SGI Itanium II facility provided by the Danish Centre for Scientific Computing and on the Linux cluster of the Institute for Computational Astrophysics. The Dark Cosmology Centre is funded by the DNRF.

REFERENCES

Górski, K. M., Banday, A. J., Hivon, E., & Wandelt, B. D. 2002, in ASP Conf. Ser. 281: Astronomical Data Analysis Software and Systems XI, ed. D. A. Bohlender, D. Durand, & T. H. Handley, 107

Inoue, A. K., Iwata, I., & Deharveng, J.-M. 2006, MNRAS, 371, L1

Kroupa, P. 1998, MNRAS, 298, 231

Leitherer, C., Schaerer, D., Goldader, J. D., Delgado, R. M. G., Robert, C., Kune, D. F., de Mello, D. F., Devost, D., & Heckman, T. M. 1999, ApJS, 123, 3

Mac Low, M.-M. & Ferrara, A. 1999, ApJ, 513, 142

Razoumov, A. O. & Sommer-Larsen, J. 2006, ApJ, 651, L89

Richards, G. T., Strauss, M. A., Fan, X., Hall, P. B., Jester, S., Schneider, D. P., Vanden Berk, D. E., Stoughton, C., Anderson, S. F., Brunner, R. J., Gray, J., Gunn, J. E., Ivezić, Ž., Kirkland, M. K., Knapp, G. R., Loveday, J., Meiksin, A., Pope, A., Szalay, A. S., Thakar, A. R., Yanny, B., York, D. G., Barentine, J. C., Brewington, H. J., Brinkmann, J., Fukugita, M., Harvanek, M., Kent, S. M., Kleinman, S. J., Krzesiński, J., Long, D. C., Lupton, R. H., Nash, T., Neilsen, Jr., E. H., Nitta, A., Schlegel, D. J., & Snedden, S. A. 2006, AJ, 131, 2766

Salpeter, E. E. 1955, ApJ, 121, 161

Sawicki, M. & Thompson, D. 2006, ApJ, 642, 653

Shapley, A. E., Steidel, C. C., Pettini, M., Adelberger, K. L., & Erb, D. K. 2006, ApJ, 651, 688

Sommer-Larsen, J. 2006, ApJ, 644, L1

Sommer-Larsen, J. & Dolgov, A. 2001, ApJ, 551, 608

Sommer-Larsen, J., Götz, M., & Portinari, L. 2003, ApJ, 596, 47